Integrating Remote Sensing and Area Frame Sampling for Rice Area Estimation: Evidence from Viet Nam*

Anthony Burgard[1], Arturo Y. Pacificador, Jr.[1], Takaaki Masaki[†1], Anna Christine Durante[1], and Pamela Lapitan[1]

[1]Asian Development Bank, Manila, Philippines

March 2, 2026

Abstract

Rice is central to food security, livelihoods, and macroeconomic stability across Asia and the Pacific, making reliable estimates of rice cultivation area critical for agricultural policy, climate risk management, and economic planning. However, administrative reporting systems may be subject to measurement error and inconsistent implementation. This paper develops a scalable and statistically defensible framework for estimating rice cultivation area by integrating satellite-based classification with a probability-based area frame survey, and demonstrates its application through a case study in Viet Nam during the 2024 summer–autumn season. We implement a stratified three-stage nested grid sampling design to generate high-quality ground truth data and enable design-based inference with transparent measures of uncertainty. Rice classification is conducted using the Japan Aerospace Exploration Agency's INAHOR system on Google Earth Engine, combining Sentinel-2 optical indices and ALOS-2 synthetic aperture radar backscatter features within a Random Forest framework. Province-level estimates from expansion, ratio, and adjusted ratio estimators converge around 2,500 km^2, with coefficients of variation below 10 percent. All survey- and satellite-based estimates exceed official administrative figures, suggesting potential underestimation in reported totals. Overall, the approach offers a scalable pathway for strengthening crop statistics using open earth observation data and probability-based sampling methods.

Keywords: rice; agricultural statistics; remote sensing; area frame sampling; Viet Nam
JEL codes: C81; C83; Q10; Q15

Conference submission: ICAS-X Conference 2026.

*The authors certify that the text, figures, tables, and all materials contained in this manuscript are original and free from any copyright violations.

[†]Corresponding author: tmasaki@adb.org

1. Introduction

Across Asia and the Pacific, where rice underpins food security, rural livelihoods, and regional trade, accurate and timely measurement of rice cultivation area is essential for monitoring agricultural production, responding to climate shocks, and producing reliable agricultural statistics for economic planning. This need is particularly salient in Viet Nam, where rice remains both a staple food and a major export commodity. In rice-dominant regions such as the Mekong Delta, exposure to flooding, drought, salinity intrusion, and land subsidence further heightens the value of seasonally responsive and spatially explicit monitoring systems. Reliable rice area statistics therefore support not only agricultural reporting functions, but also trade forecasting, disaster response planning, and climate adaptation policy [1].

Despite strong policy demand for high-frequency crop statistics, operational rice-area estimates in many settings continue to rely on administrative reporting systems. These systems typically compile local reports based on field observation and aggregation across administrative layers. While administratively comprehensive, such approaches may be vulnerable to observer bias, inconsistent implementation across localities, limited verification protocols, and logistical constraints during adverse weather. Moreover, administrative systems often do not provide transparent measures of statistical uncertainty, limiting their usefulness for risk-based policymaking and for benchmarking alternative measurement approaches.

Remote sensing offers a scalable complement to traditional compilation systems[2]. The growing availability of publicly accessible satellite imagery—including Sentinel missions, Landsat, and synthetic aperture radar (SAR) platforms—combined with cloud-based processing environments such as Google Earth Engine (GEE), has reduced barriers for producing operational crop maps. Operational systems such as Sen2-Agri and INAHOR demonstrate the feasibility of near-real-time crop monitoring at scale [3**?** –5]. Yet satellite-based classification is not an automatic substitute for statistical design. Accuracy depends on ground truth data with precise geolocation, correct timing aligned with crop phenology, and reliable labels. Without a probability-based sampling framework, training and validation data may be spatially clustered and accuracy assessment may be biased [6–8], undermining defensible inference for official statistics [9–11].

This paper presents and validates a methodology for estimating rice cultivation area in An Giang Province during the 2024 summer–autumn season by integrating (i) satellite-based classification using JAXA's International Asian Harvest mOnitoring system for Rice (INAHOR) implemented on GEE and (ii) a probability-based, grid-based area frame survey designed to generate statistically defensible ground truth labels and enable design-based inference. INAHOR combines SAR data from ALOS-2 with Sentinel-2 optical imagery within a Random Forest framework, while the area-frame survey ensures objective sample selection and supports unbiased estimation with interpretable uncertainty [5, 12].

This study makes three contributions. First, we develop and operationalize a statistically defensible, multi-stage grid-based area frame sampling design tailored to fragmented agricultural landscapes. The three-stage nested framework (1 km $\rightarrow$ 200 m $\rightarrow$ 50 m), combined with stratification across administrative districts and dominant land-use classes, supports both provincial and district-level inference while remaining operationally feasible. We formalize sample size determination around a policy-relevant precision target (CV $<$ 10%), explicitly linking variance decomposition to field allocation decisions.

Second, we integrate design-based survey inference with satellite-based classification within

a unified estimation framework. By comparing expansion, ratio, and adjusted ratio estimators alongside an INAHOR-based jackknife estimate, we clarify trade-offs between variance reduction and sensitivity to auxiliary-data mismatch. Rather than positioning remote sensing as a substitute for survey design, we demonstrate how probability-based ground truth collection and operational earth observation systems can be mutually reinforcing—combining statistical defensibility with spatial completeness [11, 13].

Third, we provide evidence on discrepancies between administrative reporting and integrated survey–remote sensing estimates of rice area. In our application, design-based and classification-based estimates exceed the administrative benchmark, motivating careful reconciliation of definitions (planted vs. harvested area), temporal alignment, and measurement protocols in official crop statistics.

2. Methods

2.1. Overview

The workflow consists of five sequential steps: (i) construct a land-cover-informed area sampling frame; (ii) draw a stratified, three-stage nested grid sample; (iii) collect field-based ground truth labels at selected segment centroids; (iv) perform rice classification using INAHOR on Google Earth Engine (GEE); and (v) estimate total rice area using design-based estimators and compare results with administrative and model-based estimates.

2.2. Area frame sampling design

Sampling frame and reclassification. We use JAXA's High-Resolution Land-Use and Land-Cover (LULC) map for Viet Nam (2020). The original classes are consolidated into four categories (rice, other crops, built-up/urban, and water bodies) to align with the field labeling protocol and to support stratification and auxiliary estimation [14].

Three-stage nested grid structure. The study area is partitioned hierarchically: Stage 1: 1 km $\times$ 1 km GRIDs (primary sampling units); Stage 2: 200 m $\times$ 200 m SUBGRIDs; Stage 3: 50 m $\times$ 50 m SEGMENTS (ultimate sampling units). Within each selected GRID, four SUBGRIDs are selected using a serpentine systematic pattern to promote spatial dispersion; within each selected SUBGRID, two SEGMENTS are selected similarly [13, 15]. The centroid of each selected segment is used as the field observation point (Figure 1).

Stratification. Stratification is implemented at the GRID level. The 11 administrative districts form primary strata to ensure coverage and enable district-level inference. Additional strata are defined for GRIDs dominated by non-rice land uses (other crops, built-up, or water), based on LULC composition thresholds, to improve representativeness in heterogeneous landscapes.

2.3. Estimation of total rice area

Let y_{ijk} denote the number of rice pixels in the k-th segment of the j-th sub-grid within the i-th grid. The total rice area estimator under the three-stage design is:

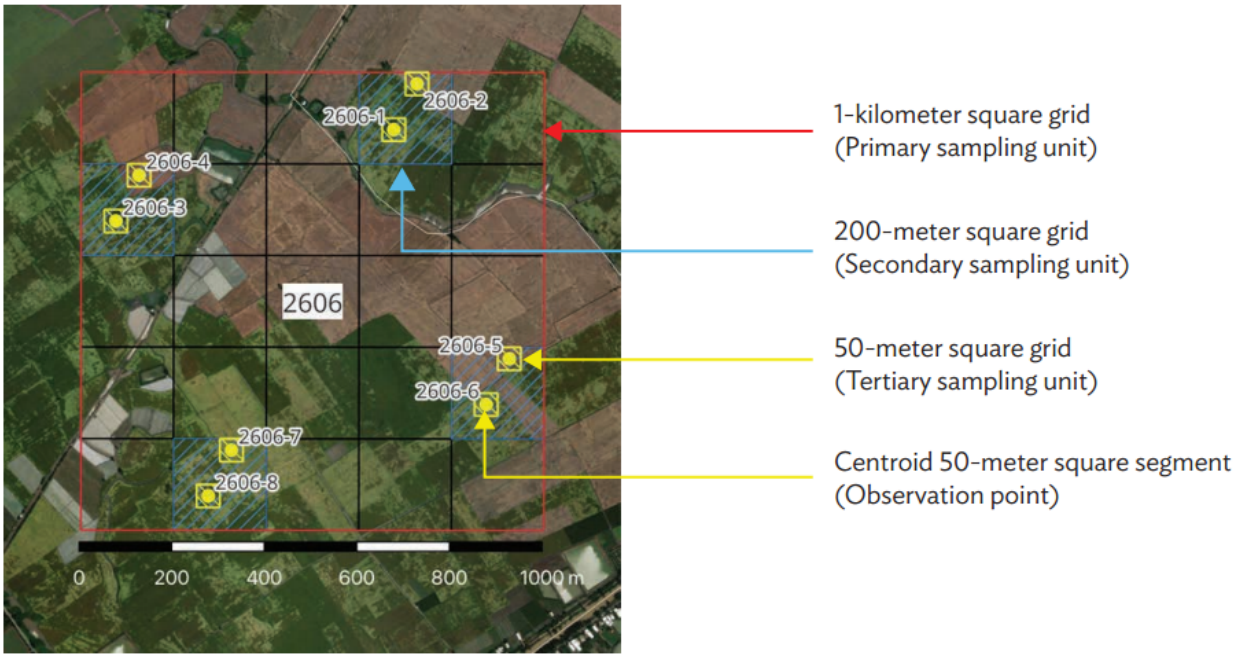

Figure 1: Illustration of the nested three-stage sampling design.

$$\hat{Y} = \frac{A}{a}\sum_{i=1}^{a}\frac{B_i}{b_i}\sum_{j=1}^{b_i}\frac{D_{ij}}{d_{ij}}\sum_{k=1}^{d_{ij}} y_{ijk} = \sum_{i=1}^{a}\sum_{j=1}^{b_i}\sum_{k=1}^{d_{ij}} w_{ijk}\, y_{ijk} \tag{1}$$

where the expansion weight is

$$w_{ijk} = \frac{A}{a} \times \frac{B_i}{b_i} \times \frac{D_{ij}}{d_{ij}}. \tag{2}$$

2.4. Variance decomposition

The variance of the three-stage expansion estimator can be written as the sum of three components, reflecting variability across GRIDs, across SUBGRIDs within GRIDs, and across SEGMENTs within SUBGRIDs:

$$\begin{aligned} V(\hat{Y}) = \underbrace{A^2\left(\frac{1}{a}-\frac{1}{A}\right)S_1^2}_{\text{Between GRIDs}} + \underbrace{\frac{A}{a}\sum_{i=1}^{A} B_i^2\left(\frac{1}{b_i}-\frac{1}{B_i}\right)S_{2i}^2}_{\text{Between SUBGRIDs within GRID}} \\ + \underbrace{\frac{A}{a}\sum_{i=1}^{A}\frac{B_i}{b_i}\sum_{j=1}^{B_i} D_{ij}^2\left(\frac{1}{d_{ij}}-\frac{1}{D_{ij}}\right)S_{3ij}^2}_{\text{Between SEGMENTs within SUBGRID}}. \end{aligned} \tag{3}$$

Here, S_1^2 denotes the variance of GRID totals across the population of GRIDs, S_{2i}^2 denotes the variance of SUBGRID totals within GRID i, and S_{3ij}^2 denotes the variance of SEGMENT totals within SUBGRID j of GRID i.

2.5. Sample size determination

We select sample size to meet a target precision threshold of $CV(\hat{Y}) < 10\%$. When between-GRID variation dominates, a simplified approximation is:

$$V(\hat{Y}) \approx A^2 \left(\frac{1}{a} - \frac{1}{A}\right) S_1^2, \tag{4}$$

where

$$S_1^2 = \frac{1}{A-1} \sum_{i=1}^{A} \left(Y_{i..} - \bar{Y}^*\right)^2, \tag{5}$$

$$Y_{i..} = \sum_{j=1}^{B_i} \sum_{k=1}^{D_{ij}} y_{ijk}, \tag{6}$$

$$\bar{Y}^* = \frac{1}{A} \sum_{i=1}^{A} Y_{i..}. \tag{7}$$

The coefficient of variation is:

$$CV(\hat{Y}) = \frac{\sqrt{V(\hat{Y})}}{\hat{Y}} \times 100\%. \tag{8}$$

In the application, $a = 34$ sampled GRIDs achieves the CV target under empirically derived variance inputs.

2.6. Ratio and adjusted ratio estimators

Ratio estimator. To improve precision, we also report a ratio estimator that leverages an auxiliary rice-area total X derived from the auxiliary land-cover product. Let x_{ijk} denote auxiliary rice pixels in segment (i, j, k) and $\hat{X} = \sum w_{ijk} x_{ijk}$. The ratio estimator is:

$$\hat{Y}_{R1} = \frac{\hat{Y}}{\hat{X}} X = \frac{\sum w_{ijk} y_{ijk}}{\sum w_{ijk} x_{ijk}} X. \tag{9}$$

The segment-level expansion weight is:

$$w_{ijk} = \frac{A}{a} \times \frac{B_i}{b_i} \times \frac{D_{ij}}{d_{ij}}. \tag{10}$$

An approximate variance estimator for $\hat{Y}_{R1}$ is:

$$s^2(\hat{Y}_{R1}) = s^2(\hat{Y}) + \hat{R}^2 s^2(\hat{X}) - 2\hat{R} s(\hat{Y}, \hat{X}), \tag{11}$$

with

$$\hat{R} = \frac{\hat{Y}}{\hat{X}}. \tag{12}$$

Adjusted ratio estimator. Auxiliary totals may be locally misaligned with ground observations due to classification differences, boundary effects, or timing mismatch. We therefore also report an adjusted ratio estimator that screens out segments with severe auxiliary matching discrepancies and recalibrates weights on the reduced sample. The estimator retains the form of equations (9)–(12), computed on the screened dataset.

The ratio estimator is sensitive to mismatches between the auxiliary land-cover map (2020) and the reference season (2024). Such discrepancies in rice extent can introduce bias, which motivates the use of the adjusted ratio estimator to identify segments with inconsistencies with auxiliary data and recalibrate weights accordingly.

2.7. INAHOR classification on GEE

Rice classification is implemented using INAHOR on Google Earth Engine (GEE), integrating Sentinel-2 optical imagery and ALOS-2 SAR imagery. From Sentinel-2 surface reflectance, INAHOR constructs vegetation- and water-sensitive indices (NDVI, NDWI, NDSI) and seasonal composites using robust aggregation to reduce cloud contamination [16, 17].

ALOS-2 HH and HV backscatter are converted to decibel scale and filtered to reduce speckle. INAHOR derives additional features (HH+HV and HH−HV) and computes temporal summary statistics (minimum, maximum, mean, and range) to capture seasonal dynamics associated with flooding, canopy development, and harvest.

The probability-sampled ground truth segments are used as labeled observations to train a Random Forest classifier (30 trees) [18]. The trained model is then applied province-wide to generate a binary rice/non-rice classification map at 50-meter spatial resolution, along with pixel-level classification probabilities that form the basis of the uncertainty surface [5, 12].

2.8. Classification accuracy assessment

Classification accuracy is evaluated using fivefold cross-validation based on the probability-sampled ground truth data. The labeled segments are randomly partitioned into five approximately equal folds. In each iteration, four folds are used for training and one fold for validation, and this process is repeated five times so that each fold serves once as the validation set. Reported metrics represent averages across the five validation runs.

Accuracy is assessed using a confusion matrix constructed at the segment level, which aligns with the sampling design and reduces spatial autocorrelation bias that may arise from pixel-level validation [9, 10]. From the confusion matrix, we compute the following standard metrics:

- **Overall accuracy (OA)**: the proportion of correctly classified segments.
- **Producer's accuracy (PA)**: the probability that a reference class is correctly classified (recall), measuring omission error.

- **User's accuracy (UA)**: the probability that a predicted class is correct (precision), measuring commission error.
- **Cohen's kappa coefficient**: a chance-corrected measure of agreement between predicted and reference classes.

Because rice/non-rice discrimination is the primary objective, class-specific metrics for rice are particularly emphasized. Producer's accuracy for rice reflects the proportion of true rice segments correctly identified, while user's accuracy for rice reflects the reliability of predicted rice segments.

To ensure consistency with the stratified sampling design, accuracy metrics can be computed using sampling weights to produce design-consistent estimates of population-level accuracy. However, cross-validation primarily evaluates predictive performance of the classifier under the observed sample, whereas design-based estimators provide unbiased inference for total rice area at the population level. The two approaches serve complementary purposes: cross-validation assesses model discrimination capacity, while probability-based sampling ensures unbiased aggregate area estimation.

2.9. Jackknife uncertainty for INAHOR

To quantify uncertainty in the INAHOR-derived total, we implement a delete-one-GRID jackknife. Let $\hat{Y}_{(i)}$ denote the INAHOR total omitting GRID i from the training sample. The jackknife mean is:

$$\hat{Y}_{JK} = \frac{1}{34} \sum_{i=1}^{34} \hat{Y}_{(i)}, \tag{13}$$

and its variance estimator is:

$$s^2(\hat{Y}_{JK}) = \frac{1}{34(33)} \sum_{i=1}^{34} \left(\hat{Y}_{(i)} - \hat{Y}_{JK}\right)^2 . \tag{14}$$

3. Data

3.1. Study area and reference season

The study covers An Giang Province in Viet Nam's Mekong Delta, using administrative boundaries consistent with the 2024 analysis period. An Giang spans approximately 3,600 km^2 and is characterized by low-lying alluvial plains, dense irrigation infrastructure, and extensive rice cultivation. Rice production typically follows three seasonal cycles: winter–spring, summer–autumn, and autumn–winter. This study focuses on the 2024 summer–autumn season, with field observations timed to coincide with late-season conditions in August 2024 [1].

3.2. Satellite data used by INAHOR

INAHOR uses PALSAR-2 ScanSAR Level 2.2 (`JAXA/ALOS/PALSAR-2/Level2_2/ScanSAR`) imagery acquired by the PALSAR-2 instrument onboard the ALOS-2 satellite, together with Sentinel-

2 multispectral imagery accessed via GEE. The PALSAR-2 Level 2.2 ScanSAR product provides terrain-corrected and radiometrically calibrated L-band synthetic aperture radar (SAR) backscatter data in HH and HV polarizations at approximately 25-meter spatial resolution, enabling cloud-penetrating, day-and-night observation of vegetation structure and surface moisture conditions. Sentinel-2 provides surface reflectance data from which optical indices such as NDVI, NDWI, and NDSI are computed across the season [5, 12].

3.3. Auxiliary land cover map

The JAXA high-resolution land-use and land-cover product for Viet Nam (2020) is used to define sampling strata, compute land-class compositions within sampling units, and provide auxiliary totals for ratio estimation. Land-cover classes are consolidated into the four-category scheme used for sampling and field labeling [14].

3.4. Ground truth field survey data

Ground truth labels were collected through field visits to the centroid of sampled 50 m × 50 m segments between 13 and 16 August 2024. A total of 34 primary sampling GRIDs were surveyed, yielding 272 observation segments (8 per GRID: 4 SUBGRIDs × 2 SEGMENTS). Enumerators recorded GPS coordinates, rice/non-rice status, estimated rice coverage within the segment, and geo-referenced photographs for verification. Data were collected using the Survey Solutions platform [19].

A total of 272 segments were collected across 34 sampled GRIDs, corresponding to 8 segments per GRID. Field teams recorded GPS coordinates, rice/non-rice labels, estimated rice coverage, and four directional photographs for each point. Due to access constraints such as flooded paddies or blocked paths, enumerators occasionally shifted the observation point within the same 50 m × 50 m segment footprint. Data were collected using the Survey Solutions platform, ensuring standardized metadata capture and geotagged photo documentation.

Field operations required occasional adjustments due to access constraints (e.g., flooded paddies or blocked paths). When necessary, observation points were shifted short distances to ensure safe access while remaining within the intended segment footprint. This ground truth dataset serves both as training/validation data for classification and as the basis for design-based estimation [9, 10].

4. Results

4.1. Rice cultivation maps and uncertainty surfaces

INAHOR produces a rice cultivation map for An Giang Province for the 2024 summer–autumn season, along with an associated uncertainty surface (Figure 2 and Figure 3). Of the province's total land area of 3,532.59 km^2, 2,511.62 km^2 (71.1%) are classified as rice and 1,020.97 km^2 (28.9%) as non-rice. The map is generated at a spatial resolution of 50 meters, and total rice area is obtained by aggregating pixels classified as rice across the province.

Spatially, the rice map reveals contiguous cultivation across low-lying alluvial plains and irrigation-connected landscapes, while non-rice areas concentrate around built-up centers, permanent water bodies, and localized zones of crop diversification. The associated uncertainty surface

is spatially structured rather than random: higher uncertainty clusters near boundaries between rice and non-rice parcels and within fragmented agricultural mosaics. These patterns are consistent with local spectral overlap in optical indices, heterogeneity in backscatter dynamics, and phenological variation during transitional growth stages.

Classification performance is evaluated using fivefold cross-validation based on the probability-sampled ground truth data. Accuracy metrics indicate strong discriminative performance. Overall accuracy is 95.3%. Producer's accuracy (recall) is 93.24% for rice and 97.18% for non-rice, indicating low omission error for both classes. User's accuracy (precision) is 96.94% for rice and 93.79% for non-rice, suggesting limited commission error. The Cohen's kappa coefficient is 0.91, reflecting a high level of agreement between the classification and reference observations beyond chance.

Taken together, the high overall accuracy, balanced producer's and user's accuracies, and strong kappa statistic indicate that the INAHOR classification achieves robust rice/non-rice discrimination in the study area. At the same time, the spatially structured uncertainty surface motivates integrating model outputs with probability-based sampling to ensure unbiased aggregate inference even when classification ambiguity is locally concentrated.

Figure 2: Rice cultivation map of An Giang Province, Summer–Autumn 2024.

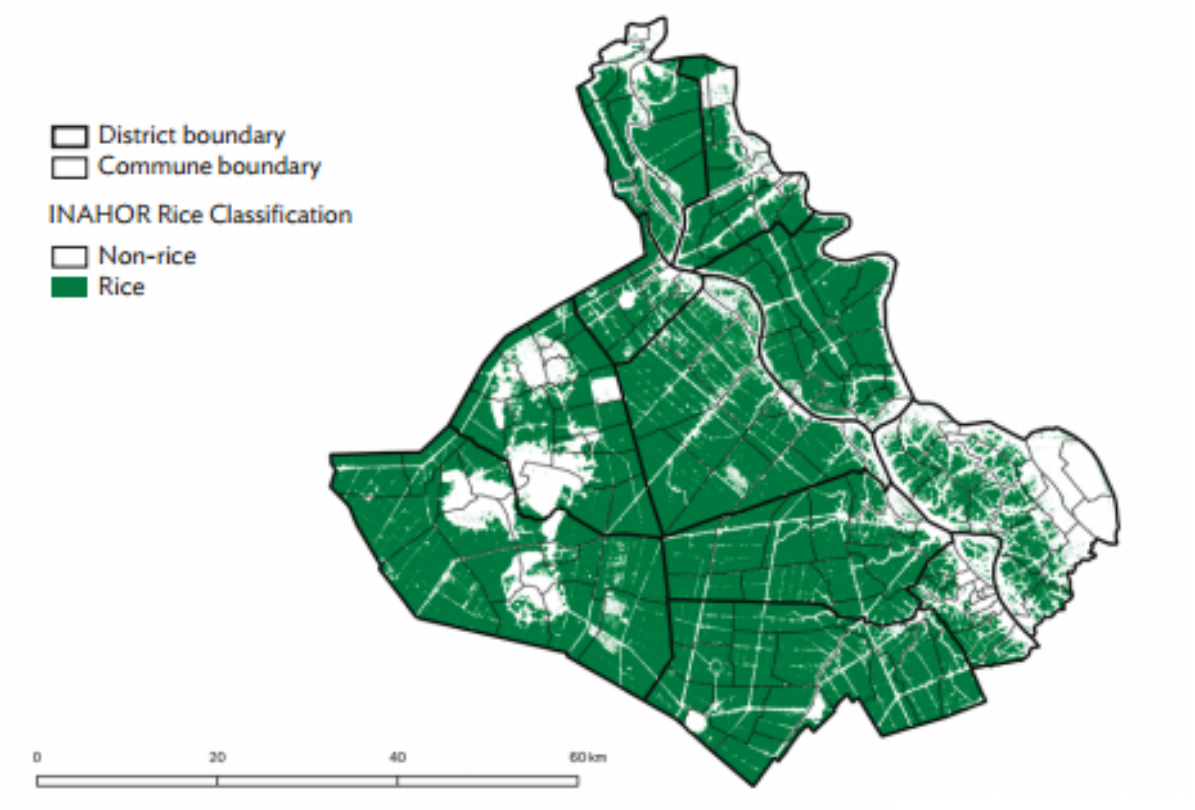

Figure 3: Classification uncertainty surface, Summer–Autumn 2024.

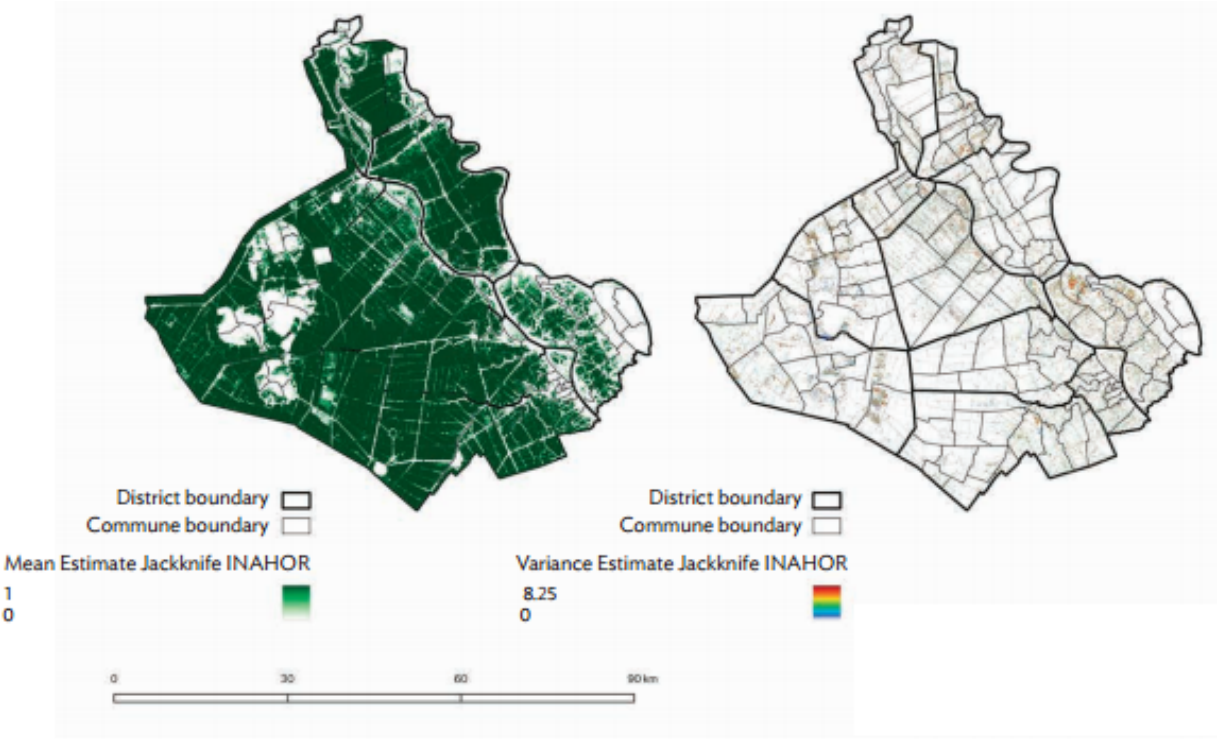

Table 1: Classification Accuracy Metrics (Fivefold Cross-Validation)

	Class	
Metric	Rice	Non-Rice
Overall accuracy	95.3%	
Producer's accuracy	93.24%	97.18%
User's accuracy	96.94%	93.79%
Cohen's kappa	0.9056	

4.2. Province-level rice area estimates across methods

Province-level rice area estimates are reported in Table 2 and visualized in Figure 4. Across methods, point estimates converge around 2,500 km^2.

The expansion estimator yields 2,517.6 km^2 with $CV = 8.04\%$, meeting the 10% precision target. The ratio estimator yields 2,444.5 km^2 with improved precision ($CV = 5.02\%$). The adjusted ratio estimator yields 2,501.1 km^2 with a substantially lower CV (0.30%). The INAHOR jackknife estimate is 2,500.1 km^2 with an estimated CV of 0.19%. The near equality of the adjusted ratio and INAHOR jackknife estimates suggests convergence between design-based inference and model-based classification once auxiliary-data mismatches are screened.

All sample- and satellite-based estimates exceed the administrative benchmark of 2,284.8 km^2 (differences of +7.0% to +10.2%). Based on design-based standard errors (Figure 4), the expansion and ratio estimators yield intervals that include the administrative benchmark, while the adjusted ratio and INAHOR jackknife estimates concentrate tightly around 2,500 km^2.

Table 2: Summary of area estimates across methods.

Estimator	Estimate (km^2)	CV (%)	Comparison with NSO (%)
Remote Sensing (INAHOR) – Jackknife	2,500.1	0.19	+9.4
Expansion Estimator	2,517.6	8.04	+10.2
Ratio Estimator	2,444.5	5.02	+7.0
Adjusted Ratio Estimator	2,501.1	0.30	+9.5
NSO Administrative Report	2,284.8	–	–

4.3. District-level heterogeneity

District-level estimates (see Appendix A) reveal substantial geographic heterogeneity in rice concentration and estimator precision. In districts where rice dominates the landscape, estimates are stable across estimators and uncertainty is relatively small. In more heterogeneous districts, dispersion across estimators increases, reflecting greater sensitivity to auxiliary-data alignment and local land-use mosaics. These results underscore the value of stratification and grid-level coverage for producing defensible sub-provincial estimates.

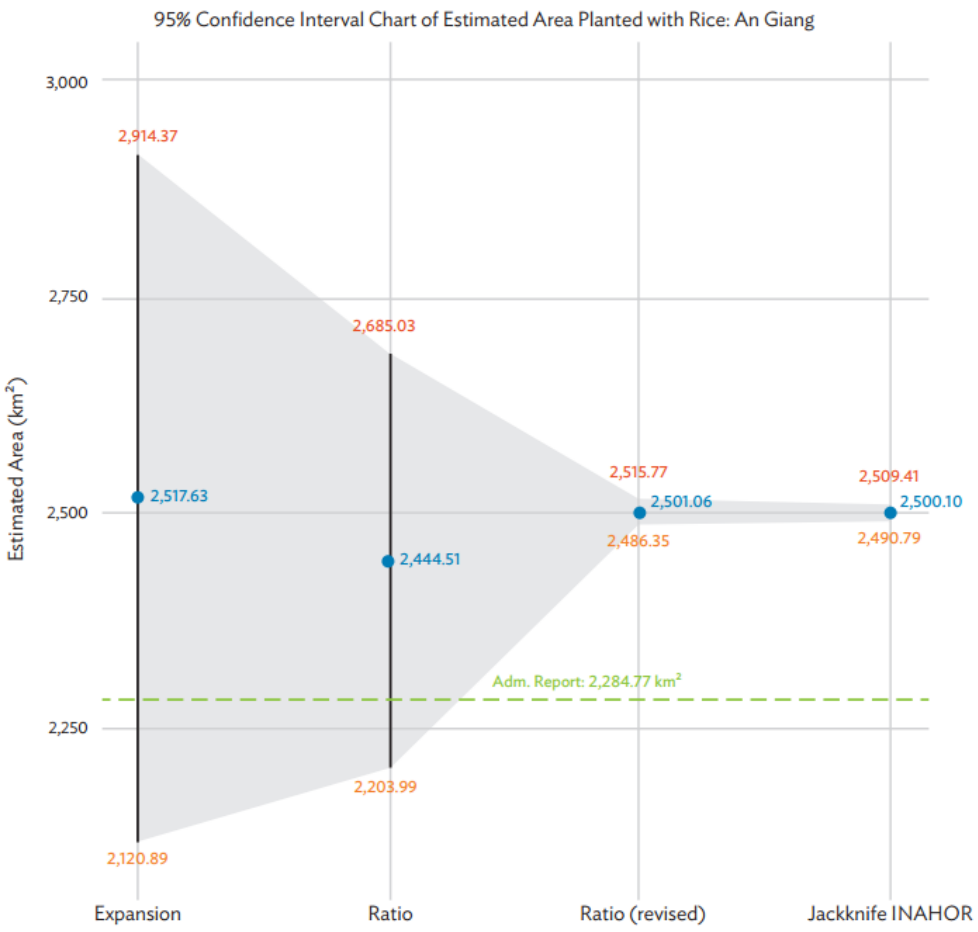

Figure 4: Province-level rice area estimates with uncertainty.

Districts with highly fragmented cropping patterns, such as Cho Moi, exhibited large dispersion across estimators and higher variance components. These patterns reflect local land-use mosaics and auxiliary data mismatches, underscoring the importance of stratification and GRID-level coverage for sub-provincial analysis.

4.4. Feature separability and seasonal dynamics

Observed feature dynamics align with agronomic expectations and support the rice/non-rice discrimination logic. Optical indices such as NDVI exhibit seasonal peaks during active growth stages, with rice observations generally exhibiting higher median NDVI than non-rice areas. Overlap increases during transitional months due to fallow periods, mixed cropping, and post-harvest conditions.

SAR-derived features display more consistent separability throughout the season, reflecting differences in surface water conditions and canopy structure in irrigated rice systems. Temporal ranges of HH and HV backscatter further improve discrimination by capturing flooding-to-canopy development dynamics. These patterns support the joint use of optical and SAR data in the Random Forest classifier.

5. Discussion

Three implications emerge. First, integrating probability-based area sampling with remote sensing enables rice area estimates with interpretable uncertainty. The grid-based area frame ensures unbiased selection of observation points across heterogeneous land-use patterns and supports design-based inference, which is central to official statistics production where uncertainty reporting and reproducibility are required [10, 11].

Second, estimator choice materially affects operational precision. Ratio estimation can reduce variance by leveraging auxiliary information, but its performance depends on the alignment between the auxiliary totals and the reference season. When auxiliary data are temporally or spatially mismatched, the adjusted ratio estimator shows how diagnostic screening and weight recalibration can substantially improve stability. More broadly, combining probability-based sampling with operational remote sensing systems offers national statistical offices a structured framework for enhancing crop statistics through independent validation, regular season-aligned monitoring, and clear measures of uncertainty, all of which are increasingly important for climate-risk management and agricultural policy.

Third, cloud-based processing lowers technical barriers but does not remove the need for high-quality field protocols. INAHOR's GEE implementation supports rapid iteration and large-area mapping, yet supervised classification performance remains sensitive to label accuracy and phenological timing. Training sample design can affect classifier performance, particularly in heterogeneous landscapes, reinforcing the value of probability-based sampling and careful field protocols [20–22].

The persistent difference between integrated estimates and administrative totals may reflect underestimation in administrative reporting, definitional differences (e.g., planted versus harvested area), or timing differences in compilation. Reconciling these requires explicit metadata alignment and targeted validation exercises, particularly in districts where discrepancies are largest.

6. Conclusion

This paper demonstrates a scalable rice area estimation framework that integrates satellite-based classification (Sentinel-2 and ALOS-2 via INAHOR on GEE) with a stratified three-stage grid area-frame survey to generate statistically defensible ground truth data and enable design-based inference. Across estimators, rice area in An Giang Province during the 2024 summer–autumn season is consistently around 2,500 km^2, with design-based CVs meeting conventional precision targets and the adjusted ratio estimator yielding the tightest uncertainty. The framework offers a practical template for strengthening crop statistics using open earth observation data and defensible field protocols, while highlighting the importance of sustained investment in ground truth quality, temporal alignment, and quality assurance systems for scaling to national production.

Appendix A. Tables of Rice Area Estimates by Province and District

Table A1: Expansion Estimator of Total Area Planted with Rice (km^2)

Province/District	Estimate	SE	CV(%)	LL	UL
An Giang	2,501.06	7.46	0.30	2,486.44	2,515.68
Thành ph Long Xuyên (883)	55.28	33.87	61.27	-15.37	125.92
Thành ph Châu Đc (884)	69.42	1.42	2.04	66.46	72.38
Huyn An Phú (886)	228.25	1.78	0.78	224.52	231.97
Th xã Tân Châu (887)	71.64	27.73	38.71	13.80	129.49
Huyn Phú Tân (888)	158.21	157.71	99.69	-170.77	487.18
Huyn Châu Phú (889)	407.13	16.38	4.02	372.96	441.31
Huyn Tnh Biên (890)	304.55	2.40	0.79	299.54	309.56
Huyn Tri Tôn (891)	460.38	49.94	10.85	356.20	564.55
Huyn Châu Thành (892)	235.41	103.18	43.83	20.18	450.64
Huyn Ch Mi (893)	63.75	21.19	33.24	19.55	107.95
Huyn Thoi Sn (894)	463.63	17.38	3.75	427.37	499.90

Table A2: Ratio Estimator of Total Area Planted with Rice (km^2) — All Sample Observations

Province/District	Estimate	SE	CV(%)	LL	UL
An Giang	2,444.51	122.77	5.02	2,203.87	2,685.14
Thành ph Long Xuyên (883)	55.33	2.72	4.91	49.67	60.99
Thành ph Châu Đc (884)	50.75	3.63	7.16	43.16	58.34
Huyn An Phú (886)	156.42	9.01	5.76	137.62	175.22
Th xã Tân Châu (887)	76.16	9.41	12.36	56.52	95.80
Huyn Phú Tân (888)	224.02	36.88	16.46	147.09	300.95
Huyn Châu Phú (889)	347.49	18.22	5.24	309.47	385.51
Huyn Tnh Biên (890)	219.29	0.08	0.03	219.13	219.45
Huyn Tri Tôn (891)	429.50	19.37	4.51	389.09	469.91
Huyn Châu Thành (892)	288.29	3.16	1.09	281.70	294.88
Huyn Ch Mi (893)	203.20	111.76	55.00	-29.93	436.33
Huyn Thoi Sn (894)	394.07	17.75	4.50	357.05	431.09

Table A3: Adjusted Ratio Estimator of Total Area Planted with Rice (km^2) — Excluding 25 Observations with Large Matching Problems

Province/District	Estimate	SE	CV(%)	LL	UL
An Giang	2,501.06	7.46	0.30	2,486.44	2,515.68
Thành ph Long Xuyên (883)	55.33	2.72	4.91	49.67	60.99
Thành ph Châu Đc (884)	74.14	1.11	1.50	71.83	76.45
Huyn An Phú (886)	154.24	1.66	1.08	150.78	157.70
Th xã Tân Châu (887)	108.58	0.73	0.67	107.07	110.09
Huyn Phú Tân (888)	244.18	0.00	0.00	244.18	244.18
Huyn Châu Phú (889)	340.89	1.94	0.57	336.85	344.93
Huyn Tnh Biên (890)	219.29	0.08	0.03	219.13	219.45
Huyn Tri Tôn (891)	464.69	0.31	0.07	464.04	465.34
Huyn Châu Thành (892)	288.29	3.16	1.09	281.70	294.88
Huyn Ch Mi (893)	144.25	0.00	0.00	144.25	144.25
Huyn Thoi Sn (894)	407.16	5.47	1.34	395.76	418.56

Table A4: Jackknife Estimator from Estimated Area Using INAHOR (km^2)

Province/District	Estimate	SE	CV(%)	LL	UL
An Giang	2,500.10	4.72	0.19	2,490.85	2,509.35
Thành ph Long Xuyên (883)	50.65	0.25	0.49	50.16	51.13
Thành ph Châu Đc (884)	73.86	0.24	0.32	73.39	74.33
Huyn An Phú (886)	151.00	0.26	0.17	150.48	151.51
Th xã Tân Châu (887)	105.51	0.35	0.33	104.83	106.20
Huyn Phú Tân (888)	241.80	0.37	0.15	241.08	242.51
Huyn Châu Phú (889)	355.95	0.82	0.23	354.34	357.57
Huyn Tnh Biên (890)	225.19	0.59	0.26	224.03	226.34
Huyn Tri Tôn (891)	476.87	0.76	0.16	475.37	478.37
Huyn Châu Thành (892)	293.30	0.34	0.11	292.64	293.96
Huyn Ch Mi (893)	127.27	1.02	0.80	125.28	129.27
Huyn Thoi Sn (894)	398.71	0.55	0.14	397.64	399.78

References

[1] National Statistics Office of Viet Nam. Statistical Yearbook of 2023. National Statistics Office of Viet Nam; 2024. Accessed 2025-06-11. Available from: https://www.nso.gov.vn/en/default/2024/07/statistical-yearbook-of-2023/.

[2] Rotairo L, et al. Use of Remote Sensing to Estimate Paddy Area and Production: A Handbook. Asian Development Bank; 2019.

[3] Defourny P, et al. Near Real-Time Agriculture Monitoring at National Scale at Parcel Resolution: Performance Assessment of the Sen2-Agri Automated System in Various Cropping Systems around the World. Remote Sensing of Environment. 2019;221:551-68.

[4] European Space Agency. Sentinels for Agricultural Statistics – Final Report. European Space Agency; 2023. Accessed 2025-06-11. Available from: https://eo4society.esa.int/wp-content/uploads/2023/02/esa-sentinels-for-agricultural-statistics.pdf.

[5] Japan Aerospace Exploration Agency. Estimation of Paddy Rice Planted Area Using Synthetic Aperture Radar – Development of Software "INAHOR"; n.d. Accessed 2025-06-11. Available from: https://www.eorc.jaxa.jp/SAFE/prototyping/accomplishments/inahor/.

[6] Congalton RG. A Comparison of Sampling Schemes Used in Generating Error Matrices for Assessing the Accuracy of Maps Generated from Remotely Sensed Data. Photogrammetric Engineering and Remote Sensing. 1988;54(5):593-600.

[7] Congalton RG. Using Spatial Autocorrelation Analysis to Explore the Errors in Maps Generated from Remotely Sensed Data. Photogrammetric Engineering and Remote Sensing. 1988;54(5):587-92.

[8] Durante AC, et al. Improving Paddy Rice Statistics Using Area Sampling Frame Technique. Asian Development Bank; 2018. 565.

[9] Congalton RG. A Review of Assessing the Accuracy of Classifications of Remotely Sensed Data. Remote Sensing of Environment. 1991;37(1):35-46.

[10] Stehman SV. Sampling Design for Accuracy Assessment of Land Cover. International Journal of Remote Sensing. 2009;30:5243-72.

[11] Gallego FJ. Remote Sensing and Land Cover Area Estimation. International Journal of Remote Sensing. 2004;25(15):3019-47.

[12] Google Earth Engine. Earth Engine Data Catalog; n.d. Accessed 2025-06-11. Available from: https://developers.google.com/earth-engine/datasets.

[13] Gandharum L, et al. Remote Sensing Versus the Area Sampling Frame Method in Paddy Rice Acreage Estimation in Indramayu Regency, West Java Province, Indonesia. International Journal of Remote Sensing. 2021;42(5):1738-67.

[14] Japan Aerospace Exploration Agency. High-Resolution Land-Use and Land-Cover Map of Vietnam for 2020 (Version 23.09); 2023. Accessed 2025-06-11. Available from: https://www.eorc.jaxa.jp/ALOS/en/dataset/lulc/lulc_vnm_v2309_e.htm.

[15] WorldCereal. WorldCereal (ESA) Website; 2025. Accessed 2025-06-11. Available from: https://esa-worldcereal.org/en.

[16] McFeeters SK. The Use of the Normalized Difference Water Index (NDWI) in the Delineation of Open Water Features. International Journal of Remote Sensing. 1996;17(7):1425-32.

[17] Takeuchi W, Yasuoka Y. Development of Normalized Vegetation, Soil and Water Indices Derived from Satellite Remote Sensing Data. Journal of the Japan Society of Photogrammetry and Remote Sensing. 2004;43(6):7-19.

[18] Belgiu M, Csillik O. Sentinel-2 Cropland Mapping Using Pixel-Based and Object-Based Time-Weighted Dynamic Time Warping Analysis. Remote Sensing of Environment. 2018;204:509-23.

[19] World Bank. Survey Solutions CAPI/CAWI platform: Release 25.01.2; 2025. Washington, DC: The World Bank.

[20] Shetty S, et al. Assessing the Effect of Training Sampling Design on the Performance of Machine Learning Classifiers for Land Cover Mapping Using Multi-Temporal Remote Sensing Data and Google Earth Engine. Remote Sensing. 2021;13(8):1433.

[21] Zhang H, et al. Comparing Three Methods of Selecting Training Samples in Supervised Classification of Multispectral Remote Sensing Images. Sensors. 2023;23(20):8530.

[22] Moraes D, et al. Influence of Sample Size in Land Cover Classification Accuracy Using Random Forest and Sentinel-2 Data in Portugal. In: 2021 IEEE International Geoscience and Remote Sensing Symposium (IGARSS). Brussels: IEEE; 2021. .